On the Effects of Nonuniform Sampling for Interferometric Phase Estimation in the Presence of Layover

F. Bordoni[†], A. Jakobsson[‡], F. Gini[†], F. Lombardini[†]

[†] Dept. of "Ingegneria dell'Informazione", University of Pisa, via G. Caruso 14, 56122 Pisa, Italy
Tel: +39-(0)50-2217-550, Fax: +39-(0)50-568-522, E-mail: {f.bordoni, f.lombardini, f.gini}@ing.unipi.it

[‡]Dept. of Electrical Engineering, Karlstad University, SE-651 88 Karlstad, Sweden
Tel: +46-(0)54-700-2330, Fax+46-(0)54-700-2197, E-mail: andreas.jakobsson@kau.se

ABSTRACT

This work tackles the problem of interferometric phase estimation in the presence of layover by using nonuniform multibaseline interferometric synthetic aperture radar systems. The effects of nonuniform sampling on Fourier-based and superresolution spectral estimation methods are investigated. The impact on both the spectral properties and on the interferometric phase estimation performance is considered. The analysis of interferometric phase estimation performance is based on Monte Carlo simulations, comparing with the corresponding Cramér Rao lower bound. The focus is on realistic single-pass acquisition systems with a low number of phase centers and a nonuniform linear array structure.

1. INTRODUCTION

Interferometric synthetic aperture radar (InSAR) is an increasingly expanding technique allowing for the estimation of three-dimensional terrain images with high spatial resolution and height accuracy [1]. The conventional InSAR system acquires two complex SAR images from two antennas slightly separated by a (single) cross-track baseline [2]. Using the phase difference between the echoes collected by the antennas at the interferometer, the so-called interferometric phase (IP), the elevation angle can be accurately determined for each pixel in the SAR images corresponding to the same area of ground. However, this technique suffers from the layover phenomenon [1]: when the imaged scene contains highly sloping areas or discontinuous surfaces, the received signal is the superposition of echoes backscattered from the various patches of terrain that are mapped in the same range-azimuth resolution cell but have different elevation angles (see Figure 1). The result is that the height map produced by the InSAR system is affected by strong distortions. A multibaseline InSAR system, i.e., a system with more than two SAR sensors, has the ability to resolve the multiple sources along the elevation angle, and several approaches based either on beamforming or superresolution techniques have been suggested in the literature [3]. An additional problem, not taken into account in the above mentioned papers, is the fact that the backscattering sources cannot be represented as point-like targets: because of their extended nature, the backscattered signal is affected by the so-called speckle phenomenon, which could be modelled as correlated complex Gaussian multiplicative noise [4]. To counteract the deleterious effects of the speckle, i.e., the phase noise and signal decorrelation, it is often advantageous to process more than one look, combining several observations of the same terrain area [2]. This was done in [4, 5, 6], where the Capon, least squares, MUSIC, RELAX, APES, and weighted subspace fitting (WSF) algorithms were extended to handle multilook data. Among these, the multilook versions of MUSIC, of RELAX (M-RELAX) and of WSF were found to be preferable, reaching comparable estimation accuracy. Overall, WSF generally provides the best interferometric phase estimation performance at a computational complexity comparable with that of root-MUSIC, which is much lower than that of M-RELAX [6]. The above mentioned approaches show satisfactory performance when a uniform linear array (ULA) structure is assumed. Such geometry allows for computationally efficient rooting algorithms and, for WSF, it is necessary to obtain a practically useful implementation. In addition to the computational aspects, irregular sampling deeply modifies the properties of spectral estimation methods, producing anomalous strong sidelobes in the beampattern and in the functional of Fourier-based spatial estimation techniques [7], making it challenging to obtain accurate elevation estimates [8, 9]. Regrettably, the ULA structure is rarely encountered in practical situations: the acquisition geometry is mostly determined by mechanical and structural considerations which are not directly related to the estimation requirements; in fact, often such considerations will rather result in a nonuniform sampling. The practical relevance of nonuniform acquisition systems and the deep effect of nonunform sampling on spectral estimation performance stress the importance to study the mechanism at the basis of nonuniform sampling influence on estimation

performance. In the past, great attention has been paid to the impact of the array geometry on the mailobe sharpness, sidelobe level and unambiguous range, in order to reach the best resolution for a given number of sensors [7]. Nevertheless, to our knowledge, the literature lacks an analysis of the effects on nonuniform sampling on supperresolution methods, such as MUSIC and RELAX, i.e., those methods which often provide the best performance in the ULA case [4]. In this paper, we analyze the effects of nonuniform sampling on the nonparametric and superreresolution spectral methods which prove to be the most effective in the ULA case. In particular, we examine a nonuniform array structure with three antennas; this is the most common array configuration for multibaseline InSAR systems of single-pass kind [10, 11]. The impact on the spectral properties and on the IP estimation performance is examined via Monte Carlo (MC) simulations.

2. DATA MODEL AND PROBLEM STATEMENT

Consider a multibaseline cross-track interferometric system, composed of a nonuniform linear array (NLA) of K two-way phase centres. The distance between the first and the last phase centres of the array is denoted as the baseline length, B. Assume that N looks are available. For look n, the pixel complex amplitudes collected from the array of sensors can be well modelled as [4]

$$\mathbf{y}(n)=\sum_{i=1}^{N_S}\sqrt{\tau_i}\,\mathbf{a}(\varphi_i)\odot\mathbf{x}_i(n)+\mathbf{v}(n)\,,\quad n=1,2,\ldots,N, \qquad (1)$$

where $\mathbf{y}(n)$, $\mathbf{a}(\varphi_i)$, $\mathbf{x}_i(n)$ and $\mathbf{v}(n)$ are K-dimensional complex vectors, τ_i is a non-negative scalar, $\odot$ is the Hadamard (elementwise) product, and N_S is the number of sources, i.e., the number of terrain patches with different elevation angles. Further, $\mathbf{v}(n)$ is a thermal noise, typically modelled as a spatially white complex Gaussian process, with zero mean and power σ_v^2. The factor τ_i is the radar reflectivity or *texture*. It is modelled as a real, positive, unknown deterministic parameter. Furthermore, $\mathbf{a}(\varphi_i)$ denotes the array steering vector of the ith source, given by

$$\mathbf{a}(\varphi_i)=\left\{\exp\left[j\,d_k\,\varphi_i/B\right]\right\}_{k=1}^{K}, \qquad (2)$$

where d_k is the distance between the kth sensor and the first one. In the sequel, the structure $[n_1\ n_2\ \cdots\ n_K]$ is used to denote an array geometry such as $n_i/n_K=d_i/B$, where $i=1,\cdots,K$. Further, φ_i is an unknown deterministic parameter representing the IP for the ith terrain patch, i.e., the phase difference between the two furthest phase centres in the array. The IP is related to the elevation angle θ_i as $\varphi_i=-4\pi B\cos(\xi-\theta_i)/\lambda$, where ξ is the tilt angle of the baseline and λ the radar wavelength, and

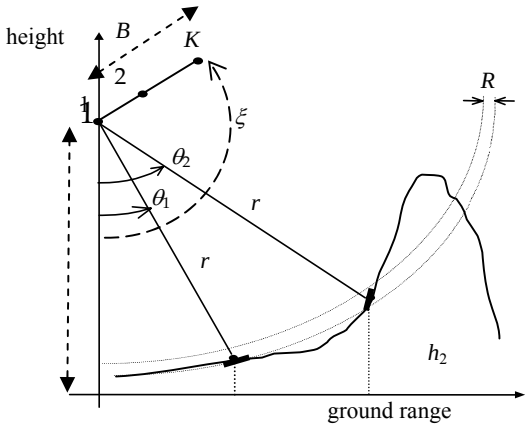

Figure 1. Geometry of the InSAR system with N_S=2 layover sources.

implicitly to the terrain height, $h_i=H-r\cos(\theta_i)$, where H is the system height and r is the range of the examined resolution cell (see also Figure 1). Finally, $\mathbf{x}_i(n)$ represents the speckle distortion affecting the ith backscattering source. It is modelled as a complex-valued correlated Gaussian process, with zero mean, unit power, and covariance matrix $\mathbf{C}_i=E\{\mathbf{x}_i(n)\mathbf{x}_i^H(n)\}$, where $E\{\cdot\}$ and $(\cdot)^H$ denote the expectation and the Hermitian transpose, respectively. For performance analysis only, we assume that the N_S vectors $\{\mathbf{x}_i(n)\}$ have a triangular-shaped spatial autocorrelation sequence [2]

$$\left[\mathbf{C}_i\right]_{k,l}=\begin{cases}1-\dfrac{\left|d_k-d_l\right|}{B}b_i & \text{for } \left|d_k-d_l\right|\le B/b_i\\ 0 & \text{otherwise}\end{cases}, \qquad (3)$$

where $b_i=B_\perp/B_{\perp ci}$ is the normalized baseline relative to the ith terrain patch and depends on the radar system parameters and on the local terrain slope, $B_\perp$ denotes the baseline orthogonal to the line of sight, and $B_{\perp ci}$ denotes the orthogonal critical baseline of the ith component, i.e., the value for which the speckle of the ith component is completely decorrelated at the extremities of the array. The goal here is to estimate the phases, $\{\varphi_i\}_{i=1}^{N_S}$, from $\{\mathbf{y}(n)\}_{n=1}^{N}$, when N_S is known and σ_v^2, $\{\tau_i\}_{i=1}^{N_S}$, and $\{\mathbf{C}_i\}_{i=1}^{N_S}$ are unknown nuisance parameters.

3. REVIEW OF SPECTRAL ESTIMATION METHODS

Beamforming is a non-parametric spectral estimation method, belonging to the class of filter-bank approach [12]. According to it, the data vector is processed by a complex FIR filter, $\mathbf{h}_B$, of length K. Assumed a spatially white ($\mathbf{R}_y=\mathbf{I}$) input, the filter is designed in order to pass undistorted the

signals with IP φ while attenuating all the other components as much as possible. Thus, the beamforming functional is given by the power spectral density (PSD) of the output of the filter [12]

$$\mathbf{P}_B(\varphi) = \mathbf{h}_B^H(\varphi)\,\mathbf{R}_y\mathbf{h}_B(\varphi) = \frac{\mathbf{a}^H(\varphi)\mathbf{R}_y\,\mathbf{a}(\varphi)}{K^2},\ \varphi \in \mathrm{UR}, \quad (4)$$

where UR denotes the IP unambiguous range and $\mathbf{R}_y$ is the theoretical data covariance matrix. The IPs are estimated from the location of the N_S highest peaks of the functional in (4), where $\mathbf{R}_y$ is replaced by a consistent estimate of $\mathbf{R}_y$, say $\hat{\mathbf{R}}_y$. The resolution properties of beamforming are analogous to those of the *periodogram*. This sets the conventional Fourier (or Rayleigh) resolution limit at $\Delta\varphi = 2\pi(K-1)/K$ [12].

The Capon beamformer is a non-parametric, data-dependent spectral estimation method belonging to the class of filter-bank approaches. The Capon filter, $\mathbf{h}_C(\varphi)$, is designed under the same constraints used for beamforming, but considering the general case of spatially correlated signals. The Capon functional, expressed as a function of the IP, is given as [12]

$$\mathbf{P}_C(\varphi) = \frac{1}{\beta}\left(\frac{1}{\mathbf{a}^H(\varphi)\mathbf{R}_y^{-1}\,\mathbf{a}(\varphi)}\right),\ \varphi \in \mathrm{UR}, \quad (5)$$

where β is the bandwidth of Capon filter. The Capon functional provides a PSD estimate generally more accurate than that obtained by beamforming [12]. The IPs are estimated as the location of the N_S highest peaks of (5), where $\mathbf{R}_y$ is replaced by $\hat{\mathbf{R}}_y$ [12].

M-RELAX is an extension to the multi-look scenario of RELAX algorithm. It is a parametric technique which estimates amplitude and frequency of complex signals, by fitting the observed data vector to the desired signal [4]. The estimates are obtained by an iterative procedure, which at the end minimizes the cost function [4]

$$Q_N(\boldsymbol{\alpha}(n), \varphi) = \frac{1}{N}\sum_{n=1}^{N}\left\| \mathbf{y}(n) - \sum_{i=1}^{N_S}\alpha_i(n)\mathbf{a}(\varphi_i)\right\|^2, \quad (6)$$

where $\|\cdot\|$ is the Euclidean norm, $\boldsymbol{\alpha}(n)$ the vector which collects the source amplitudes, $\{\alpha_i(n)\}_{i=1}^{N_S}$. At each step, say q, M-RELAX assumes $N_S = q$ and repeats iteratively the successive minimization of the cost functions [4]

$$Q_{N\,q\,m}(\boldsymbol{\alpha}(n), \varphi) = \frac{1}{N}\sum_{n=1}^{N}\left\| \mathbf{y}_m(n) - \sum_{i=1}^{q}\alpha_i(n)\mathbf{a}(\varphi_i)\right\|^2, \quad (7)$$

with respect to $\{\alpha_m(n), \varphi_m\}$, where $m = 1, 2, \cdots, q$,

$$\mathbf{y}_m(n) = \mathbf{y}(n) - \sum_{i=1,\, i\neq m}^{q}\hat{\alpha}_i(n)\mathbf{a}(\hat{\varphi}_i), \quad (8)$$

is the residual data vector and $\{\hat{\alpha}_i(n), \hat{\varphi}_i\}_{i=1,\, i\neq m}^{q}$ are the amplitudes and the IP estimates, assumed to be given (typically from a previous iteration). Minimization of (7) is given by

$$\hat{\varphi}_m = \arg\max\{\mathbf{a}^H(\varphi)\hat{\mathbf{R}}_y^m\mathbf{a}(\varphi)\}, \quad (9)$$

$$\hat{\alpha}_m = \frac{\mathbf{a}^H(\hat{\varphi}_m)\mathbf{y}_m(n)}{K}, \quad (10)$$

where $\hat{\mathbf{R}}_y^m$ is the sample covariance matrix estimate of the residual data vector, $\mathbf{y}_m(n)$ [4]. It is worth noting that the IP estimate, $\hat{\varphi}_m$, obtained at each step from (9) is the location of the highest peak of the beamforming functional relative to the residual vector in (8). This fact, as explained in Section 4, is of key importance to understand how nonuniform sampling affects the IP estimation performance of M-RELAX.

MUSIC is a parametric method designed for frequency estimation of exponential signals embedded in additive white noise. The MUSIC functional is given by [12]

$$\mathbf{P}_M(\varphi) = \frac{1}{\mathbf{a}^H(\varphi)\mathbf{G}\mathbf{G}^H\mathbf{a}(\varphi)}, \quad (11)$$

where $\mathbf{G}$ is the matrix collecting the $(K - N_S)$ eigenvectors of $\mathbf{R}_y$ corresponding to the $(K - N_S)$ least dominating eigenvalues. The IP estimates are obtained as the locations of the N_S highest peaks of the estimated functional in (11), where $\mathbf{G}$ is replaced by $\hat{\mathbf{G}}$, obtained from the eigendecomposition of $\hat{\mathbf{R}}_y$.

4. NONUNIFORM SAMPLING EFFECTS

In order to understand the effect of nonuniform sampling on the IP estimation accuracy, it is useful to analyze the expression of the functional of beamforming, Capon and MUSIC, and to develop a comparison between the ULA and NLA scenario. Consider a full ULA with $K_f = 4$ phase centres, here denoted ULA(4), and the corresponding *thinned* NLA, with $K = 3$ phase centres and structure $[0\,2\,3]$, here denoted NLA(3), which has the same aperture and the same minimum spatial lag as the ULA(4) system. We note that the NLA(3) is the typical structure for multibaseline InSAR systems of single-pass kind [10, 11]. The comparison is particularly appropriate because the two array geometries are characterized by the same UR [13]. For sake of clarity and without loss of generality, assume completely correlated multiplicative noise, i.e., $\{b_i = 0\}_{i=1}^{N_S}$ [14]. Under these assumptions, and the beamforming functional in (4), for the NLA(3) and the ULA(4) becomes

$$\mathbf{P}_B(\varphi)=\frac{3}{K^2}\sigma_v^2+\sum_{i=1}^{N_S}\frac{\tau_i}{K^2}\left[\frac{1}{2}\cos\left(\frac{\varphi-\varphi_i}{3}\right)\right]$$
$$+\sum_{i=1}^{N_S}\frac{\tau_i}{K^2}\left[\frac{1}{2}\cos\left(\frac{2}{3}(\varphi-\varphi_i)\right)+\frac{1}{2}\cos(\varphi-\varphi_i)\right] \quad (12)$$
$$+\left\{\frac{\sigma_v^2}{K^2}+\sum_{i=1}^{N_S}\frac{\tau_i}{K^2}\left[\cos\left(\frac{\varphi-\varphi_i}{3}\right)+\frac{1}{2}\cos\left(\frac{2}{3}(\varphi-\varphi_i)\right)\right]\right\}$$

where the terms between curly brackets are equal to zero for the NLA(3). Note that (12) shows that the NLA expression of the beamforming functional associated to each single source has a higher sidelobe level than the corresponding full ULA expression. This reduction of the main-to-side lobe ratio is well visible in Figure 2, which represents the functional for $N_S=1$. Figure 2 also highlights the effect of nonuniform sampling on the Capon and MUSIC functionals. In the NLA case, the Capon functional has sidelobes located in correspondence of those of the standard beamformer, which are not present in the ULA case, whereas the NLA MUSIC functional is less sharp than the ULA functional. The presence of anomalous sidelobes in the NLA functionals can dangerously affect IP estimation performance in presence of layover. In fact, in the presence of multiple sources, for critical source separations, $\Delta\varphi$, the inflated sidelobes sum up, producing high spurious peaks in the functionals where no sources are actually located. This situation is depicted in Figure 3 for $N_S=2$.

In order to understand how this phenomenon affects the IP estimation accuracy, a brief numerical analysis of the performance of the spectral estimation methods described in Section 3, applied to the ULA(4) and NLA(3) data, is reported. In particular, where not otherwise stated, all the numerical results are derived assuming $N_S=2$, $N=32$, $b_1=b_2=0.2$, $SNR_1=SNR_2=12\,\text{dB}$ and $\Delta\varphi=\varphi_2-\varphi_1=315^\circ$. The data covariance matrix is estimated using the forward-only approach [12]. Estimation performance is measured in terms of root mean square error (RMSE),

$$RMSE(\hat{\varphi}_i)=\min_j\sqrt{E\{(\hat{\varphi}_i-\varphi_j)^2\}},\ i,\ j=1,2,\cdots,N_S, \quad (13)$$

where the error $(\hat{\varphi}_i-\varphi_j)$ is evaluated modulus the UR. Here, the RMSE is estimated by means of 10^3 MC runs. A comparison between the RMSE with the square root of the CRLB, derived in [14] for the NLA case, is also provided. Figures 4 and 5 show the estimation performance of the standard beamformer, Capon, MUSIC and M-RELAX for the full ULA(4) and for the corresponding thinned NLA(3), respectively. The RMSE is computed as a function of the IP difference, $\Delta\varphi$. Only half of the total UR, $[-540°, 540°]$, is shown as the performance is symmetric on the other half. Figure 4 shows that the best resolution is achieved by M-RELAX and MUSIC. Moreover, when the sources are sufficiently separated all the methods are almost unbiased and have a RMSE close to the CRLB. In the NLA(3) case, shown in Figure 5, the estimation accuracy has the same trend, except for a critical phase interval, i.e., source separation, where the performance of MUSIC and M-RELAX degrade dramatically.

A comparison between the behavior of the IP estimation performance and of the 3rd (spurious) peak of the beamformer and Capon functionals is further provided: Figure 6 reports the (normalized) amplitude and the occurrence frequency of the 3rd highest peak of each functional versus $\Delta\varphi$. Here, the occurrence frequency of the 3rd highest peak is measured by means of 10^3 MC trials, as the ratio between the number of times a 3rd peak is present and the total number of trials. Figure 6 shows that the range of $\Delta\varphi$ characterized by the largest amplitude and by unitary occurrence frequency of the 3rd peak is the same where the anomalous strong degradation of MUSIC and M-RELAX occurs. This critical behavior can be explained by Figure 3, which reports the beamformer, Capon and MUSIC functionals when the two sources have an IP difference which turns out in the superimposition of the sidelobes of the two sources. In this scenario, a strong spurious peak appears in the functionals. Figure 3 has been obtained by using the theoretical data covariance matrix; in this case the spurious peak is weaker than the true IP peaks. Nevertheless, when the covariance matrix estimate is not very accurate, the spurious peak can be even stronger than the true ones, producing an erroneous IP estimation. This phenomenon affects more dramatically MUSIC than Capon or the standard beamformer, producing the observed anomalous loss of performance of MUSIC.

As regards to M-RELAX, the loss of performance is still related to the presence of anomalous strong sidelobes, but in a slightly different way. As remarked in Section 3, at each step M-RELAX estimates the source IP as the location of the highest peak of beamforming functional [4]. It is interesting to note that beamforming does not show a loss of performance when M-RELAX degrade. As a consequence, what happens is not that the spurious peak is exchanged for a source, but for critical source separations, the strong sidelobe of each source fully superimposes to the mainlobe of the other source, generating an inflated mainlobe. The inflation of the mainlobe produces an erroneous overestimation of the amplitude of the first component at the first step of M-RELAX. When the component with the overestimated amplitude is subtracted from the data, the spectral properties of the residual data vector are completely distorted. This phenomenon is described in Figure 7, which is relative to a critical scenario, $\Delta\varphi=355^\circ$. It shows that after the subtraction of the overestimated first component, computed in the very first step of M-RELAX iterative procedure (denoted Step 1 in the figure), the second component cannot be correctly identified anymore and the remaining iterative procedure is corrupted [14]. In the figure, step 2.1 indicates the initially estimated component, and Step 2.2 the remaining residual.

Finally, it is worth remarking that the reported analysis evidences that the IP estimation methods which provide the best resolution performance, i.e., MUSIC and M-RELAX, are also the most sensitive to nonuniform sampling effects. Possible

robust NLA estimation methods will be subject of future development (see also [14]).

5. REFERENCES

[1] P. A. Rosen, S. Hensley, I. R. Joughin,F. K. Li, S. N. Madsen, E. Rodriguez, R. M. Goldstein, "Synthetic aperture radar interferometry," *IEEE Proc.*, Vol. 88, No. 3, March 2000, pp. 333 – 382.

[2] E. Rodriguez, J. M. Martin, "Theory and Design of Interferometric Synthetic Aperture Radars," *IEE Proceedings-F*, Vol. 139, No. 2, April 1992, pp. 147-159.

[3] J. Homer, I. D. Longstaff, G. Callaghan, "High Resolution 3-D SAR via Multi-Baseline Interferometry," *Proc. of the IEEE Int. Geoscience and Remote Symposium*, Lincoln, Nebraska, 1996, pp. 796-798.

[4] F. Gini, F. Lombardini, M. Montanari, "Layover solution in multibaseline SAR interferometry", *IEEE Trans. on Aerospace and Electronic Systems*, Vol. 38, No. 4, Oct. 2002, pp. 1344–1356.

[5] F. Gini, F. Lombardini, "Multilook APES for multibaseline SAR interferometry", *IEEE Trans. on Sig. Proc.*, Vol. 50, No. 7, July 2002, pp. 1800 – 1803.

[6] A. Jakobsson, F. Lombardini, F. Gini, "Weighted subspace fitting of interferometric phases for multibaseline SAR interferometry," *Proc. of the 7th Int. Symp. on Sig. Proc. and Its Applications*, 2003, Vol. 1, July 1-4, 2003, pp. 32 –324.

[7] H. L. Van Trees, *Optimum Array Processing. Part IV of Detection, Estimation, and Modulation Theory*, John Wiley & Sons, 2002, Chapter 7, pp. 827-841.

[8] A. Reigber, A. Moreira, "First Demonstration of Airborne SAR Tomography using Multibaseline L-band Data," *IEEE Trans. on Geosci. and Remote Sensing*, Vol. 38, No. 5, September 2000, pp. 2142-2152.

[9] G. Fornaro, F. Lombardini, F. Serafino, "First Experiments of Adaptive 3D SAR Tomography with Repeat-Pass Spaceborne Data," *Proc. of EUSAR '04,* Ulm, GE, May 2004.

[10] H. Fiedler, G. Krieger, F. Jochim, M. Kirschner, A. Moreira, "Analysis of bistatic configurations for spaceborne SAR interferometry," *Proc. of EUSAR '02*, Cologne, GE, June 2002, pp. 29-32.

[11] L. Rössing, J. Ender, "Multi-Antenna SAR Tomography Using Super Resolution Techniques," *Proc. of EUSAR '00*, Munich, GE, 23-25 May 2000, pp. 55-58.

[12] P. Stoica and R. Moses, *Introduction to Spectral Analysis,* Prentice Hall, Englewood Cliffs, NJ, 1997.

[13] F. Lombardini, "Optimum absolute phase retrieval in three-element SAR interferometer**,"** *IEEE Electronics Letters*, Vol. 34, No. 15, 23 July 1998, pp. 1522-1524.

[14] F. Bordoni, A. Jakobsson, F. Gini, F. Lombardini, "Nonuniform Linear Array InSAR Systems: Effect of the Irregular Sampling on Interferometric Phase Estimation," *Technical Report, University of Karlstad*, EE-2004-02, ISSN 1652-7968, Karlstad, Sweden, September 2004.

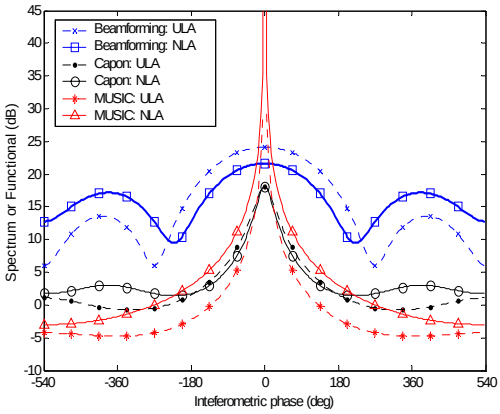

Figure 2. *Ns*=1: beamforming's, Capon's and MUSIC's functional for the ULA(4) and the NLA(3).

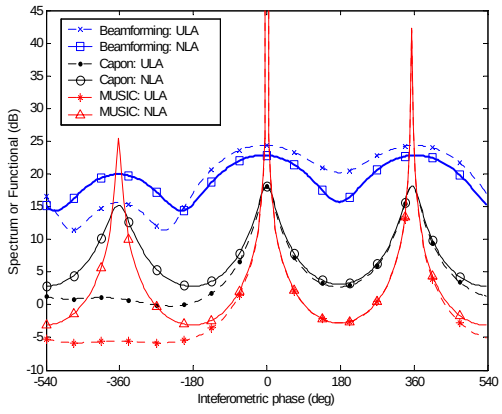

Figure 3. *Ns*=2: beamforming's, Capon's and MUSIC's functional for the ULA(4) and the NLA(3).

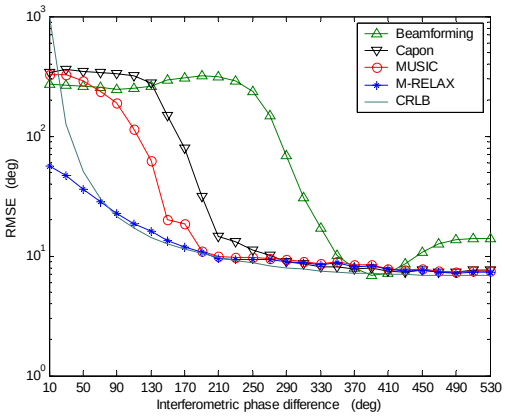

Figure 4. Estimation performance for the ULA(4) as a function of $\Delta\varphi$.

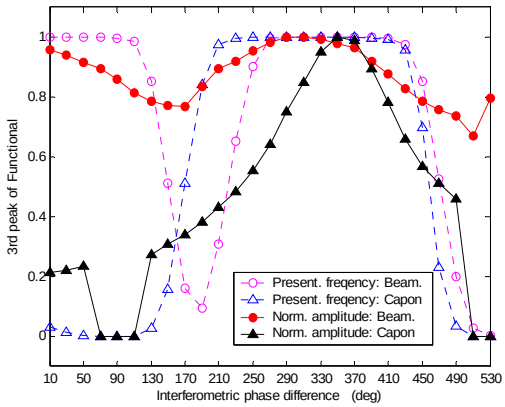

Figure 6. NLA(3): occurrence frequency and normalized amplitude of the 3rd peak of the functionals.

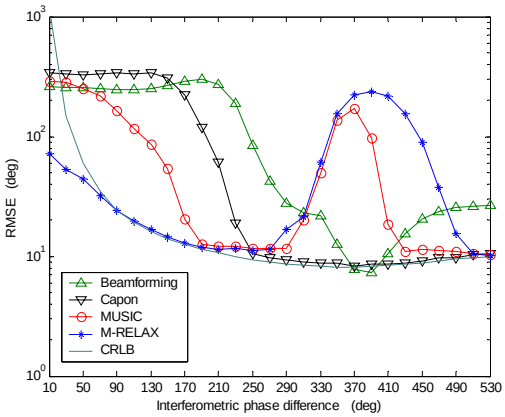

Figure 5. Estimation performance for the NLA(3) as a function of $\Delta\varphi$.

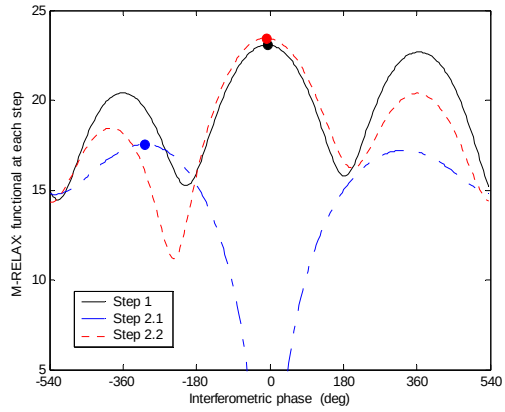

Figure 7. NLA(3). $\boldsymbol{\varphi}$=[0° 355°]. M-RELAX iterative procedure: beamforming functional computed at each step. The maximum of the functional, corresponding to the interferometric phase estimation at each step is marked by symbol ●.